Robust Load Frequency Control for Power System Considering Transmission Delay and Sampling Period

Xing-Chen Shangguan, *Student Member, IEEE,* Chuan-Ke Zhang, *Senior Member, IEEE,* Yong He, *Senior Member, IEEE,* Li Jin, *Student Member, IEEE,* Lin Jiang, *Member, IEEE,* Joseph W. Spencer, Min Wu, *Fellow, IEEE*

***Abstract*—Uncertain transmission delays and sampling periods, parameters uncertainties regarding the power system, load fluctuations, and the intermittent generation of renewable energy sources (RESs) will significantly influence a power system's frequency. This paper designs a robust delay-dependent PI-based load frequency control (LFC) scheme for a power system based on sampled-data control. First, a sampled-data-based delay-dependent LFC model of power system is constructed. Then, by applying the Lyapunov theory and the linear matrix inequality technique, a novel stability criterion is developed for the LFC of the power system by considering the sampling period and transmission delay of the communication network, which ensures that the proposed scheme operates in large sampling periods and under transmission delays. Next, an exponential decay rate (EDR) is introduced to guide the design of a robust PI-based LFC scheme. The LFC scheme with robustness is designed by setting a small EDR. The values of EDR are adjusted by the given robust performance evaluation conditions of parameter uncertainties and H_∞ performance. Finally, case studies are carried out based on a one-area power system and a three-area power system with RESs. Simulation results show that the proposed LFC scheme performs strong robustness against parameter uncertainties regarding the power system and communication network, load fluctuations, and the intermittent generation of RESs.**

***Index Terms*—Power system, Load frequency control, Sampled-data control, Robust PI controller, Transmission delay**

This work was supported in part by the National Natural Science Foundation of China under Grants 61873347 and 62022074, by the Hubei Provincial Natural Science Foundation of China under Grants 2019CFA040, by the 111 project under Grant B17040, by the Program of China Scholarship Council under Grants 201706410012 and 201706410037, and by the Fundamental Research Funds for National Universities, China University of Geosciences (Wuhan). *(Corresponding author: Chuan-Ke Zhang)*

X.C. Shangguan and L. Jin are with the School of Automation, China University of Geosciences, Wuhan 430074, China, with Hubei Key Laboratory of Advanced Control and Intelligent Automation for Complex Systems, Wuhan, 430074, China, with Engineering Research Center of Intelligent Technology for Geo-Exploration, Ministry of Education, Wuhan, 430074, China, and also with the Department of Electrical Engineering and Electronics, University of Liverpool, Liverpool L69 3GJ, United Kingdom. (email: star@cug.edu.cn; jinli@cug.edu.cn)

C.K. Zhang, Y. He, and M. Wu are with the School of Automation, China University of Geosciences, Wuhan 430074, China, with Hubei Key Laboratory of Advanced Control and Intelligent Automation for Complex Systems, Wuhan, 430074, China, and also with Engineering Research Center of Intelligent Technology for Geo-Exploration, Ministry of Education, Wuhan, 430074, China. (email: ckzhang@cug.edu.cn; heyong08@cug.edu.cn; wumin@cug.edu.cn)

L. Jiang and J. W. Spencer are with the Department of Electrical Engineering and Electronics, University of Liverpool, Liverpool L69 3GJ, United Kingdom.(email: Ljiang@liv.ac.uk; joe@liverpool.ac.uk)

I. Introduction

Load frequency control (LFC) aims at maintaining frequency and power interchanges with neighbourhood areas at scheduled values in an interconnected power system to supply reliable electric power [1, 2]. A traditional LFC employs dedicated communication channels to transmit measurements and control signals. As pointed out in Ref. [3], communication faults or cyber-attacks may stop or suspend the service of LFC. Additionally, no matter how fast or advanced the communication technology is that is used in communication network, communication fault or cyber-attacks cannot be inevitable. The data packet loss caused by communication fault or cyber-attacks is equivalent to transmission delays.

With the penetration of intermittent renewable energy sources (RESs) and the increased interaction with the demand-side response, a power system becomes a larger scale and geographically distributed system [4]. An effective future electricity market tends to employ an open communication infrastructure to support the increasingly decentralized property of control services [5, 6], such as a third-party LFC service [7]. Compared to the dedicated communication channels, open communication networks are preferred for the modern LFC scheme as they are low-cost and flexibility [5]. However, due to the usage of open communication network, some new problems are introduced into the LFC scheme, including the dropout of data packets and transmission delays [8, 9]. These problems will degrade the dynamic performance or may even cause instability of a network-based power system.

To deal with the above problems, first, a robust LFC scheme was proposed against communication network constraints [10, 12]. As an improvement, Jiang *et al.* treated data packet dropout and/or disordering as time-varying and random delays [3]. Then, based on the Lyapunov theory, the authors investigated the delay-dependent stability and the robust PID-type controller design for the LFC scheme. Further study can be found in Refs. [13, 14]. It is noted that the task mode in a continuous manner is a common assumption in the works mentioned above, *i.e.*, all data packets are transmitted over the shared communication networks without the data updating and processing. However, there is a typical updating period (sampling period) of $2-4$s for the control updating period in a practical power system, as noted in Refs. [2, 15]. Additionally, there are burdens of communication and computation since

that some microprocessors with limited computing capability and energy resources may be used in the LFC scheme [16] and the bandwidth constraints exist in the practical communication network among generation units [17]. This may result in power system instability and fault [18]. Luo *et al.* explored the impacts of the transmission delays and sampling periods on the stability of LFC [19]. Therefore, it is desirable to design an effective LFC scheme, which takes both the transmission delay and the sampling period fully into account to ensure the stability of the LFC of the power system and reduce the communication and computational burden.

Recently, a way of changing the trigger mechanism of data transmission called an event-triggered communication scheme [20] has been introduced to handle the above-mentioned problem. The event-triggered communication scheme has been implemented in a network-based power system in Refs. [16, 21–23]. In such scheme, the sampled data are only transmitted when a preset threshold condition is violated [24]. Another way is to increase the sampling period based on time-triggered sampled-data control [25, 26]. Dahiya *et al.* obtained a larger sampling period for an isolated hybrid power system with the aid of the Lyapunov theory [27]. Similarly, a larger sampling period was derived to lower the communication channel occupation and less signal transmission for a single-area power system and multi-area power system with wind power [15]. As noted in Ref. [28], the computational burden is increased in the event-triggered mechanism, due to the continuous checking of an event-triggered condition. Additionally, the implementation is difficult since extra hardware is required. Therefore, this paper focuses on the more straightforward second method to get the maximum sampling period to reduce the amount of data packet.

On the other hand, as the generation mix continues to change from large synchronous plants to smaller, decentralized RESs, the modern power system is facing new challenges [4, 29], such as stability issues, uncertainties and low inertia. In Ref. [15], a discrete and fast load frequency control is proposed to address the problem of low inertia for a power system with wind power. However, for a power system with RESs, the load change, the intermittent generation of RESs, and the uncertainties of the parameters will significantly influence the system frequency [30, 31]. Thus, an LFC with a better robustness performance is requested. Recently, some robust LFC schemes have been implemented in power system based on advanced control methods, such as sliding mode control [22, 32], active disturbance rejection control [33], model-based control [9] and model predictive control [34]. However, most of these advanced methods suggest complex state feedback or high-order dynamic controllers. As noted in [35], the industries still prefer the conventional PID-type LFC controllers. Additionally, these advanced LFC schemes do not consider either the effects of the sampling period or the transmission delay at the design stage of a robust LFC.

Motivated by the above discussions, this paper proposes a robust delay-depended PI-based LFC scheme for a power system based on sampled-data control. It is an extensive study on the work of Ref. [15]. The main contributions of this paper are summarized as follows:

- Compared to the schemes proposed in Refs. [10, 12, 15], the LFC scheme designed in this paper considers both the sampling period and transmission delay of communication network parameters in the power system based on sampled-data control. With the aid of the Lyapunov theory, the stability criterion is developed for a given controller. The stability criterion is used to calculate margins of the sampling period and transmission delay, within which the stability of the power system equipped with the given controller is guaranteed. Furthermore, under a given transmission delay, the obtained margin of the sampling period is used to increase the sampling period in the communication network to reduce communication network burden. Such a method is easier to calculate and implement than the event-triggered communication scheme proposed in [16, 21].
- Different from the complex state feedback or high-order dynamic controllers in Refs. [9, 15, 22, 32–34], a simple PI-based LFC scheme is suggested to implement robustness against disturbances and the uncertainties of the parameters. Such a scheme reduces the measurements of system state information and is more convenient for LFC of a large-scale power system.
- To cope with the uncertainties of parameters of the power system and the communication network, load, and generation of RESs, the exponential decay rate (EDR) is introduced as a performance index to guide a PI controller with robustness. Parameter uncertainties and H_∞ performance analysis conditions are given to evaluate the designed robust controller to guarantee the desired performances.

The remainder of the paper is organized as follows. Section II gives the dynamic model of sampled-data based delay-depended LFC for a multi-area power system with RESs. The stability analysis and the robust PI controller design of the LFC scheme are introduced in section III. In Section IV, case studies based on a one-area power system and a three-area power system with RESs verify the proposed scheme's effectiveness. The conclusions are drawn in Section V.

Notations: Throughout this paper, $P > 0$ (≥ 0) means that P is a real symmetric and positive-definite (semi-positive-definite) matrix; I and 0 represent the identity matrix and a zero matrix, respectively; the superscript T represents the transpose, the superscript -1 represents the inverse, and $diag\{\cdots\}$ stands for a block-diagonal matrix; the notation $*$ always denotes the symmetric block in a symmetric matrix. Moreover, for any square matrix A, we define $Sym(A) = A + A^T$. If the dimensions of matrices are not explicitly stated, they are assumed to have compatible dimensions for algebraic operations.

II. Dynamic Model of Sampled-Data-Based LFC Scheme for a Power System with RESs

In this section, a dynamical model of LFC for the power system with RESs is developed by considering the sampling period and transmission delay.

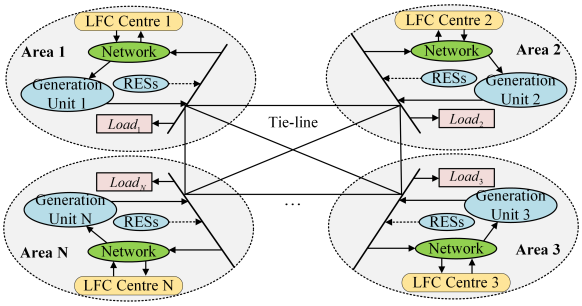

Fig. 1. Simplified diagram of N-area power system

A. An open-loop dynamic model of multi-area LFC with RESs

The block diagram for an N-area power system is shown in Fig. 1. Each area has similar structure, as shown in Fig. 2. Additionally, each control area consists of an LFC centre, generation units, and load, and may comprise RESs.

ACE in such scheme is defined as follows:

$$ACE_i = \beta_i \Delta f_i + \Delta P_{tie-i} \tag{1}$$

where β_i represents frequency bias factor; Δf_i is the deviation of frequency; and ΔP_{tie-i} represents the tie-line power exchange. For simplicity, the turbines of each generation are all assumed to be non-reheated. When the power system comprises RESs, i.e., wind power and/or solar power, these two distributed sources may have high-order dynamical frequency response models. Nevertheless, low-order dynamical models considered in this paper are sufficient for investigating frequency control issues [31], as shown in Fig. 2, where T_{RESi} is the integral time constant of RESs in area i. The state variable of ΔP_{RESi} is introduced into power system model. Based on Fig. 2, the state-space model of control area i of traditional LFC scheme can be obtained as [2]

$$\begin{cases} \dot{\tilde{x}}_i(t) = \tilde{A}_i \tilde{x}_i(t) + \tilde{B}_i u_i(t) + \tilde{F}_i \omega_i(t) \\ \tilde{y}_i(t) = \tilde{C}_i \tilde{x}_i(t) \\ \tilde{z}_i(t) = \tilde{C}_{zi} \tilde{x}_i(t) \end{cases} \tag{2}$$

where

$$\tilde{x}_i^T = [\Delta f_i \Delta P_{tie-i} \Delta P_{m1i} \cdots \Delta P_{mni} \Delta P_{v1i} \cdots \Delta P_{vni} \Delta P_{RESi}]$$

$$u_i = \Delta P_{Ci}, \tilde{y}_i = ACE_i, \tilde{z}_i = \Delta f_i, \omega_i = [\Delta P_{di} \ v_i \ \Delta P_{WSi}]^T$$

$$\tilde{A}_i = \begin{bmatrix} \hat{A}_i & \hat{A}_{12i} \\ 0 & \frac{-1}{T_{RESi}} \end{bmatrix}, \tilde{B}_i = \begin{bmatrix} \hat{B}_i \\ 0 \end{bmatrix}, \tilde{F}_i = \begin{bmatrix} \hat{F} & 0 \\ 0 & \frac{1}{T_{RESi}} \end{bmatrix}$$

$$\hat{A}_i = \begin{bmatrix} A_{11i} & A_{12i} & 0 \\ 0 & A_{22i} & A_{23i} \\ A_{31i} & 0 & A_{33i} \end{bmatrix}, \hat{B}_i = \begin{bmatrix} 0 \\ 0 \\ B_{3i} \end{bmatrix}, \hat{F}_i = \begin{bmatrix} \frac{-1}{M_i} & 0 \\ 0 & -2\pi \\ 0 & 0 \end{bmatrix}$$

$$A_{11i} = \begin{bmatrix} -\frac{D_i}{M_i} & -\frac{1}{M_i} \\ 2\pi \sum_{j=1, j\neq i}^{N} T_{ij} & 0 \end{bmatrix}, A_{12i} = \begin{bmatrix} \frac{1}{M_i} \cdots \frac{1}{M_i} \\ 0 \ \cdots \ 0 \end{bmatrix}$$

$$\hat{A}_{12i} = \begin{bmatrix} \frac{1}{M_i} & 0 \end{bmatrix}^T, A_{22i} = -A_{23i} = diag\left\{ \frac{-1}{T_{ch1i}} \cdots \frac{-1}{T_{chni}} \right\}$$

$$A_{31i} = \begin{bmatrix} \frac{-1}{R_{1i} T_{g1i}} \cdots \frac{-1}{R_{ni} T_{gni}} \\ 0 \ \cdots \ 0 \end{bmatrix}^T, A_{33i} = diag\left\{ \frac{-1}{T_{g1i}} \cdots \frac{-1}{T_{gni}} \right\}$$

$$B_{3i} = \begin{bmatrix} \frac{\alpha_{1i}}{T_{g1i}} & \cdots & \frac{\alpha_{ni}}{T_{gni}} \end{bmatrix}^T, \tilde{C}_i = [\beta_i \ 1 \ 0 \ 0]$$

$$\tilde{C}_{zi} = [1 \ 0 \ 0 \ 0], v_i = \sum_{j=1, j\neq i}^{N} T_{ij} \Delta f_j.$$

and ΔP_{mki} and ΔP_{vki} are the generator mechanical output and the valve position, respectively. $M_i, D_i, T_{gki}, T_{chki}, R_{ki}$ represent the moment of inertia of generator unit, generator unit damping coefficient, the time constant of the governor, the time constant of the turbine, and speed droop of area i, respectively. ΔP_{di} is the load disturbances of area i, α_{ki} represents the participation factor of generator k in area i, T_{ij} is the tie-line synchronizing coefficient between area i and area j, and ΔP_{RESi} and ΔP_{WSi} represent the output power change of RESs and the change of wind speed and/or solar radiation in area i, respectively. In a non-competitive environment, α_{ki} is usually fixed based on generating unit capacity and the dispatch center's requirement, while it is actually time-dependent variable and will be determined dynamically based on bid prices, availability, congestion problems, costs, and other related issues in a competitive environment [2].

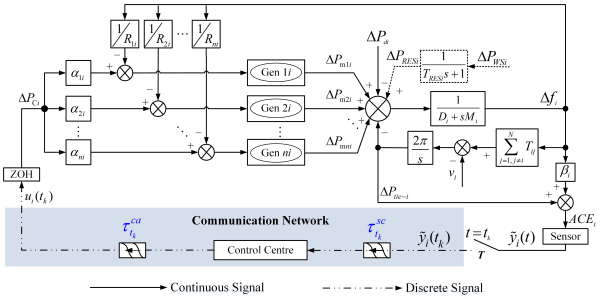

Fig. 2. Structure of control area i of N-area LFC scheme

B. Sampled-data-based LFC

Similar to Ref. [16], the following PI-type controller can be chosen as an LFC:

$$\begin{cases} \tilde{y}_i(t) = ACE_i(t) \\ u_i(t) = K_{Pi} \tilde{y}_i(t) + K_{Ii} \int \tilde{y}_i(t) dt \end{cases} \tag{3}$$

However, in sampled-data-based control loop, only sampled measurements of output signal $\tilde{y}_i(t)$ can be used for LFC scheme, that is, we only have the measurements $\tilde{y}_i(t_k)$ at sampling instant t_k. As shown in Fig. 2, the communication network is subject to network-induced delays $\tau_{t_k} = \tau_{t_k}^{sc} + \tau_{t_k}^{ca} \leq \tau_M < \infty$, where τ_M is a known constant. It is assumed that the sampling instants t_k $(k = 0, \ 1, \ 2, \cdots)$ satisfy

$$0 = t_0 < t_1 < \cdots < t_k < \cdots < \lim_{k\to\infty} t_k = +\infty \tag{4}$$

$$\Delta k = t_{k+1} - t_k = h_k \leq h_M \tag{5}$$

where h_M represents maximum acceptable sampling period. Then, under consideration of the effect of sampling and delays of the communication networks, the attainable $\tilde{y}_i(t)$ at the LFC controller can be obtained as

$$\tilde{y}_i(t) = \tilde{y}_i(t_k), \ t \in \left[t_k + \tau_{t_k}, \ t_{k+1} + \tau_{t_{k+1}} \right) \tag{6}$$

Based on (3) and (6), for $t \in \left[t_k + \tau_{t_k}, t_{k+1} + \tau_{t_{k+1}} \right)$, a feasible LFC under the network environments is designed as

$$u_i(t) = u_i(t_k) = K_{Pi} \tilde{y}_i(t_k) + K_{Ii} \int \tilde{y}_i(t_k) dt \tag{7}$$

The following virtual vectors $x_i(t) = [\tilde{x}_i^T(t) \int \tilde{y}_i^T(t) dt]^T$ and $y_i(t) = [\tilde{y}_i^T(t) \int \tilde{y}_i^T(t) dt]^T$ are defined, and equations

(2) and (7) are combined. Then, the closed-loop system with parameters uncertainty can be rewritten as

$$\begin{cases} \dot{x}_i(t) = A_i x_i(t) + B_i K_i C_i x_i(t_k) + F_i \omega_i(t) \\ y_i(t) = C_i x_i(t),\ t \in \left[t_k + \tau_{t_k}, t_{k+1} + \tau_{t_{k+1}}\right) \\ z_i(t) = C_{zi} x_i(t) \end{cases} \tag{8}$$

where

$$A_i = \begin{bmatrix} \tilde{A}_i & 0 \\ \tilde{C}_i & 0 \end{bmatrix}, B_i = \begin{bmatrix} \tilde{B}_i \\ 0 \end{bmatrix}, C_i = \begin{bmatrix} \tilde{C}_i & 0 \\ 0 & 1 \end{bmatrix}, F_i = \begin{bmatrix} \tilde{F}_i \\ 0 \end{bmatrix}$$

and $C_{zi} = [\tilde{C}_{zi}\ 0]$, $K_i = [K_{Pi}\ K_{Ii}]$.

Generally, in many cases it is very difficult, if not impossible, to obtain the accurate value of some system parameters. For $\pm\epsilon\%$ deviations from nominal values of $T_{gki}, T_{chki}, T_{RES}$, one can obtain the following uncertain LFC model.

$$\begin{cases} \dot{x}_i(t) = (\bar{A}_i + f(t)\Delta\bar{A}_i)x_i(t) + (\bar{B}_i + f(t)\Delta\bar{B}_i)u_i(t) + F_i\omega_i(t) \\ y_i(t) = C_i x_i(t) \\ z_i(t) = C_{zi} x_i(t) \end{cases} \tag{9}$$

where

$$\bar{A}_i = \begin{bmatrix} A_{11i} & A_{12i} & 0 & \hat{A}_{12i} & 0 \\ 0 & \epsilon_1 A_{22i} & \epsilon_1 A_{23i} & 0 & 0 \\ \epsilon_1 A_{31i} & 0 & \epsilon_1 A_{33i} & 0 & 0 \\ 0 & 0 & 0 & \frac{-\epsilon_1}{T_{RESi}} & 0 \\ [\beta_i\ 1] & 0 & 0 & 0 & 0 \end{bmatrix}, \Delta\bar{B}_i = \begin{bmatrix} 0 \\ \epsilon_2 B_{3i} \\ 0 \\ 0 \end{bmatrix}$$

$$\Delta\bar{A}_i = \begin{bmatrix} 0 & 0 & 0 & 0 & 0 \\ 0 & \epsilon_2 A_{22i} & \epsilon_2 A_{23i} & 0 & 0 \\ \epsilon_2 A_{31i} & 0 & \epsilon_2 A_{33i} & 0 & 0 \\ 0 & 0 & 0 & \frac{-\epsilon_2}{T_{RESi}} & 0 \\ 0 & 0 & 0 & 0 & 0 \end{bmatrix}, \bar{B}_i = \begin{bmatrix} 0 \\ \epsilon_1 B_{3i} \\ 0 \\ 0 \end{bmatrix}.$$

and $\epsilon_1 = \frac{1}{(1-\epsilon\%)(1+\epsilon\%)}$, $\frac{\epsilon\%}{(1-\epsilon\%)(1+\epsilon\%)}$, $f(t) \in [-1, 1]$.

It is noted that the decentralized control strategy is applied to the LFC scheme for the N-area power system. The interactions between different areas, *i.e.*, v_i, are treated as disturbances in the above models. Hence, the design of the multi-area LFC is divided into the repetitive design of various single-area. Additionally, the control signals of power commands sent to generators are computed by their own LFC centre in each area and independent in each area.

III. Sampled-data-based delay-dependent LFC

In this section, based on the normal sampled-data-based LFC model (8), we will first derive a stability condition of LFC considering the transmission delay and the sampling period of measurements and control signals. Then, based on the criterion and robust performance analysis conditions, a design method of the robust PI LFC scheme is introduced.

A. Stability and robust performance analysis

To design a robust PI LFC scheme, the following stability condition is first introduced:

Theorem 1: Consider system (8) with $\omega(t) = 0$. For given sampling period h_M, time delay τ_M and controller gains K_i, if there are symmetric matrices P_2, Z and $X = \begin{bmatrix} X_1 + X_1^T & -X_1 - X_2 \\ * & X_2 + X_2^T \end{bmatrix}$, and symmetric positive definite matrices P_1, P_3, and any appropriately dimensioned matrices L and M such that the following conditions hold:

$$\Xi_1 = \psi_1 + \Gamma + h_M \psi_2 < 0 \tag{10}$$

$$\Xi_2 = \begin{bmatrix} \psi_1 + \Gamma & -h_M \Phi_2^T M \\ * & -h_M Z \end{bmatrix} < 0 \tag{11}$$

where

$$\begin{aligned} \psi_1 =& Sym\left\{ \begin{bmatrix} e_1 \\ e_3 \end{bmatrix}^T P_1 \begin{bmatrix} e_5 \\ e_4 \end{bmatrix} + \Phi_2^T M(e_1 - e_2) \right\} \\ & - \begin{bmatrix} e_3 \\ e_2 \end{bmatrix}^T X \begin{bmatrix} e_3 \\ e_2 \end{bmatrix} + \begin{bmatrix} e_1 \\ e_5 \end{bmatrix}^T P_2 \begin{bmatrix} e_1 \\ e_5 \end{bmatrix} - \begin{bmatrix} e_3 \\ e_4 \end{bmatrix}^T P_2 \begin{bmatrix} e_3 \\ e_4 \end{bmatrix} \\ & + \tau_M e_5^T P_3 e_5 - \tfrac{1}{\tau_M}(e_1 - e_3)^T P_3 (e_1 - e_3) \\ \Gamma =& Sym\{\Phi_1^T L(e_5 - A_i e_1 - B_i K_i C_i e_2)\} \\ \psi_2 =& e_4^T Z e_4 + Sym\left\{ \begin{bmatrix} e_3 \\ e_2 \end{bmatrix}^T X \begin{bmatrix} e_4 \\ 0 \end{bmatrix} \right\} \\ e_l =& [0_{r\times(l-1)r} \quad I_r \quad 0_{r\times(5-l)r}], l = 1, \cdots, 5 \\ \Phi_1 =& [e_1^T \quad e_2^T \quad e_5^T]^T,\ \Phi_2 = [e_1^T \quad \ldots \quad e_5^T]^T \end{aligned}$$

and r is the dimension of matrix A in system (8). Then, system (8) is asymptotically stable for any sampling periods smaller than h_M and any delays smaller than τ_M. The proof is shown in Appendix A.

Remark 1: In Refs. [3], the sampling period is considered as a time delay, combined with a transmission delay to guide the design of the controller, while only the sampling period is considered directly to the designed controller in Refs. [9, 15]. Compared to these study, the theorem proposed can simultaneously develop the upper bounds of the sampling period and the transmission delay when the controller parameters are given.

To evaluate the robustness of the controller obtained against sampling period and transmission delay, an algorithm to find the margins of the acceptable sampling period and allowable transmission delay is shown as the following Algorithm 1.

Algorithm 1: Find the maximum sampling period h_M and maximum transmission delay τ_M for a known controller.

Step 1: Assume transmission delay is a known constant τ_k

Step 2: 1)Initialize the search interval $[h_{min}, h_{max}]$ with $h_{min} = 0$ and large enough number h_{max} and select the accuracy coefficient $h_{ac} = 0.01$.
2) Determine whether the system has a test sampling period given as $h_{test} = (h_{min} + h_{max})/2$ by checking the feasibility of LMIs (10) and (11).
3) If (10) and (11) are feasible, set $h_{min} = h_{test}$; else, set $h_{max} = h_{test}$.
4) If $|h_{min} - h_{max}| \leq h_{ac}$, obtain the $h_M = h_{min}$ and $\tau_M = \tau_k$; else, repeat 2).
5) End. Output h_M and τ_M.

Remark 2: The sampling periods and the transmission delays are coupled with the variable matrices in LMIs. Under a given controller, we fix the sampling period (or the transmission delay), and then use the above algorithm to find the maximal value of the transmission delay (or the sampling period). The fixed value and the obtained maximal value of the other are set to the margins of the sampling period and transmission delay.

To evaluate the robustness of the given controller, the following parameter uncertainties and H_∞ performance analysis conditions are introduced based on Theorem 1.

Condition 1: Consider uncertain system (9) with $w(t) = 0$. For $\exists\ \sigma > 0$, such that the following inequalities hold:

$$\Pi_1 = \begin{bmatrix} \Xi_1 & \Phi_1^T L & \sigma[e_1^T \ e_2^T][N_1 \ N_2]^T \\ * & -\sigma I & 0 \\ * & * & -\sigma I \end{bmatrix} \tag{12}$$

$$\Pi_2 = \begin{bmatrix} \Xi_2 & \begin{bmatrix} \Phi_1^T L \\ 0 \end{bmatrix} & \begin{bmatrix} \sigma[e_1^T \ e_2^T][N_1 \ N_2]^T \\ 0 \end{bmatrix} \\ * & -\sigma I & 0 \\ * & * & -\sigma I \end{bmatrix} \tag{13}$$

then, the system is robust stable against parameter uncertainties within $\pm\epsilon\%$ of T_{gki}, T_{chki} and T_{RES} for any sampling periods smaller than h_M and any delays smaller than τ_M, where $N_1 = \Delta\bar{A}_i$, $N_2 = \Delta\bar{B}_i K_i C_i$, and the other matrix notations are same as the Theorem 1 except that $A_i = \bar{A}_i$ and $B_i = \bar{B}_i$. The proof is shown in Appendix B.

Condition 2: Consider system (8) with $\omega(t) \neq 0$. For given $\gamma > 0$, such that the following inequalities hold:

$$\Pi_3 = \begin{bmatrix} \Xi_1 & -\Phi_1^T L F_i \\ * & -\gamma I \end{bmatrix} \tag{14}$$

$$\Pi_4 = \begin{bmatrix} \Xi_2 & \begin{bmatrix} -\Phi_1^T L F_i \\ 0 \end{bmatrix} \\ * & -\gamma I \end{bmatrix} \tag{15}$$

then, the system is robust stable and has an H_∞ performance index γ against non-zero disturbance $\omega(t)$ for any sampling periods smaller than h_M and any delays smaller than τ_M, where $e_1^T C_{zi}^T C_{zi} e_1$ is added into ψ_1 and the other matrix notations are same as the Theorem 1. The proof can be found in Ref. [21].

B. Design of a PI-type LFC scheme

To design a PI controller with robustness performance, EDR is introduced. The following theorems are developed.

Theorem 2: Consider system (8) with $\omega(t) = 0$. For given sampling period h_M, time delay τ_M, EDR λ and tuning parameters a and b, if there are symmetric matrices $\hat{P}_2$, $\hat{Z}$ and $\hat{X}$, and symmetric positive definite matrices $\hat{P}_1$, $\hat{P}_3$, and any appropriately dimensioned matrices $\hat{S}$, $\hat{M}$ and Y such that LMIs the following inequalities hold,

$$\hat{\Xi}_{1j} = \hat{\psi}_1 + \hat{\Gamma}_j + h_M \hat{\psi}_2 < 0 \tag{16}$$

$$\hat{\Xi}_{2j} = \begin{bmatrix} \hat{\psi}_1 + \hat{\Gamma}_j & -h_M \hat{\Phi}_1^T \hat{M} \\ * & -h_M \hat{Z} \end{bmatrix} < 0 \tag{17}$$

then system (8) is exponentially stable with an EDR for any sampling periods smaller than h_M and any delays smaller than τ_M and a feedback gain can be calculated by

$$K_i = Y(\hat{S}^T)^{-1} C_i^T (C_i C_i^T)^{-1}. \tag{18}$$

where $j = 1, 2$ and $\hat{\Gamma}_j = \hat{\Phi}_1^T \Phi_3 (\hat{S}^T e_5 - (A_i + \lambda I)\hat{S}^T e_1 - \rho_j B_i Y e_2)$ with $\Phi_3 = [I; aI; bI]$, $\rho_1 = e^{\lambda \tau_M}$ and $\rho_2 = e^{\lambda(\tau_M + h_M)}$. The other parameters are given in Theorem 1 with superscript $\hat{}$. The proof is given in Appendix C.

The EDR is introduced as a performance index to represent the control performance of a controller. It reflects the robustness and frequency response dynamic performance of a designed controller. It belongs to the domain $[0, \infty)$. The smaller the EDR, the stronger the robustness, but the worse the frequency response dynamic performance. When the EDR is set to 0, the PI controller is considered to be the strongest robust but the worst dynamical. To design a controller with the desired robustness, the following subsection is introduced based on the above conditions 1 and 2.

C. The procedure of designing a PI controller with desired robustness

For a given allowable transmission delay τ_M and a sampling period h_M, the following Algorithm 2 is described to design a controller with desired robustness, including parameter uncertainties ϵ_g and H_∞ performance γ_g.

Algorithm 2: Find λ and derive robust controller gain K

Step 1: Initialize system parameters, set τ_M, h_M, ϵ_g and γ_g.
Step 2: Initialize the search interval $[\lambda_{min}, \lambda_{max}]$ with $\lambda_{min} = 0$ and large enough number λ_{max} and select the accuracy coefficient $\lambda_{ac} = 0.001$.
Step 3: Determine whether the system has a test EDR given as $\lambda_{test} = (\lambda_{min} + \lambda_{max})/2$ by checking the feasibility of LMIs (16) and (17).
Step 4: If (16) and (17) are feasible, calculate K_{test} by equation (18). Then, bring K_{test} into Condition 1 with ϵ_g and Condition 2 with γ_g, respectively. If LMIs (12)-(15) are feasible, set $\lambda_{min} = \lambda_{test}$; else, set $\lambda_{max} = \lambda_{test}$. If (16) and (17) are not feasible, set $\lambda_{max} = \lambda_{test}$.
Step 5: If $|\lambda_{min} - \lambda_{max}| \leq \lambda_{ac}$, obtain the EDR $\lambda = \lambda_{min}$ and record $K = K_{test}$; else, repeat Step 3.
Step 6: End. Output λ and K.

IV. Case Studies

In this section, to illustrate the principle of the proposed LFC scheme, case studies are carried out based on a one-area LFC scheme, and a three-area LFC scheme with RESs.

A. One-area power system

Parameters of a one-area power system are reported in Ref. [12]. Assume that the allowable sampling period and transmission delay are set to 1 s and 3 s, respectively. By setting $a = 0$, $b = 2.03$, $\lambda_{max} = 1$, $\epsilon_g = 40$, $\gamma_g = 20$, and following Algorithm 2, we can obtain the PI controller gains $[K_P \ K_I]$=[-0.0183 -0.0453] (named as C_1) and $\lambda = 0.150$. To show the necessity of considering both transmission delay and sampling period to design a robust controller, the proposed LFC scheme is compared to the other three LFC schemes, including the fast and discrete state-feedback LFC scheme considering sampling period in Ref. [15], the robust PID-type LFC scheme considering neither sampling period nor transmission delay in Ref. [12], and the improved LMI based PID-type LFC scheme considering neither sampling period nor transmission delay in Ref. [35]. Their controller gains are given in Table I.

1) Delay margin and robust performance analysis: Using the method given in Algorithm 1, the margins of transmission delay for a one-area LFC scheme with four controllers under $h = 0.1$ s, 1 s and 2 s are calculated in Table I, where '-' represents no feasible solution. Additionally, for the given four controllers, the maximal acceptable parameter uncertainties ϵ_{max} and minimal H_∞ performance index γ are obtained under $h = 0.1$ s based on conditions 1 and 2, and shown in Fig. 3. Table I shows that the controller designed in this paper can

withstand greater time delay under the same sampling period. In contrast, the controller C_3 and C_4 considering neither the time delay nor the sampling period can only tolerate small time delay. Moreover, as seen in Fig. 3, all four control schemes can provide excellent robust performance under smaller delays, while the designed controller can tolerate greater parameter uncertainty and provide smaller H_∞ performance with the increase of time delay ($\tau > 3$s).

TABLE I
MARGINS OF TRANSMISSION DELAY FOR ONE-AREA LFC SCHEME WITH DIFFERENT CONTROLLERS UNDER SAMPLING PERIODS $h = 0.1$ S, 1 S, 2 S

Sampling periods	h=0.1s	h=1s	h=2s
C_1=−[0.0186 0.0453][this paper]	13.183	12.597	12.011
C_2=−[0.0622 0.1231 0.0226 0.1723][15]	3.320	2.734	2.050
C_3=−[0.4306 0.6356 0.1832][12]	0.195	-	-
C_4=−[1.5 3.15 0.31][35]	0.072	-	-

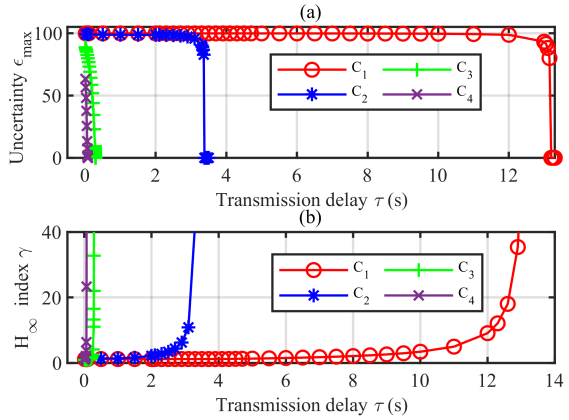

Fig. 3. Maximal uncertainty index ϵ and minimal H_∞ perform index γ with respect to delay τ under $h = 0.1$ s for one area LFC scheme

2) Simulation verification: The system equipped with the above four controllers is tested in the presence of step change of load disturbance, *i.e.*, $\Delta P_d = 0.06$ pu for $t \geq 0$. Under different communication environments, responses of the frequency deviation Δf are shown in the Fig. 4. It can be seen that C_1 proposed in this paper can remain basically identical control performance in four communication environments, while C_2-C_4 can only maintain control performance under a small sampling period and transmission delay.

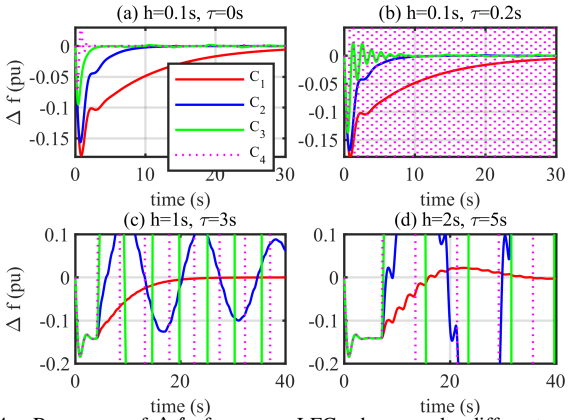

Fig. 4. Responses of Δf of one-area LFC scheme under different sampling periods and delays

3) Test of reducing communication burden: To show the effectiveness of saving the communication resources, we compared the increasing sampling period based on the time-triggered method (TTM) and the event-triggered method (ETM) proposed in Ref. [28] in the one-area power system. The transmission delay is set to 3 s. When the system subjected to random load disturbances, as shown in Fig. 5 (a), frequency responses of one-area power system with controller C_1 are illustrated in Fig. 5 (b) under TTM and ETM. Additionally, the number of signal transmission is given in Table II. It can be seen from Fig. 5 (b) that the frequency responses are almost identical under ETM ($h = 0.05$ s, $h = 0.1$ s and $h = 2$ s) and TTM ($h = 2$ s). In Table II, when ETM is used, and the sampling period is set to small values ($h <= 0.1$ s), the number of signal transmission is more than those under TTM ($h = 2$ s). However, if ETM is used when the sampling period is set to a large one ($h = 2$ s), this will further reduce the signal transmission times.

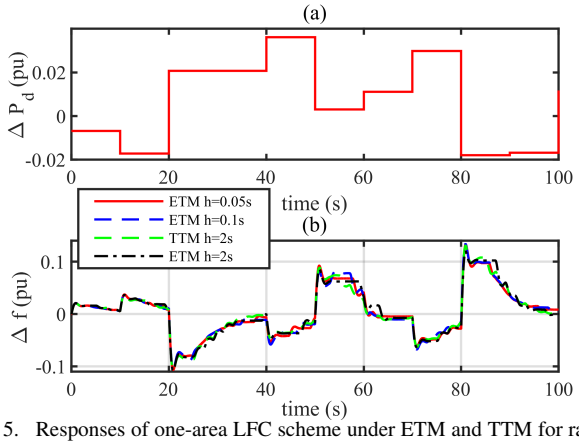

Fig. 5. Responses of one-area LFC scheme under ETM and TTM for random load disturbances. (a) random load disturbances. (b) frequency responses.

Moreover, a one-area power system with EVs is considered, and the parameters of this system are given in Case B in Ref. [21]. Setting $\tau_M = 0.3$ s, $h_M = 5.1$ s, $\lambda_{max} = 1$, $\epsilon_g = 20$, $\gamma_g = 20$, and following Algorithm 2, we can obtain the PI controller gains $[K_P\ K_I]$=-[0.0460 0.2366] (named as C_{51}) and $\lambda = 0.1$. The sampling period margin $h_M = 5.1$ s obtained is larger than the average sampling periods of 1.1327 s (obtained in Ref. [16]) and 1.9355 s (obtained in Ref. [21]) based on event-triggered scheme. Furthermore, When the sampling period is set to $h_M = 11.6$ s, we can obtain $[K_P\ K_I]$=-[0.0157 0.0804] (named as C_{52}) and $\lambda = 0.03$. The use of such a large sampling period can effectively reduce the number of signal transmissions. When the system is equipped with controllers C_{51} and C_{52} under sampling period $h = 5.1$ s and $h = 11.6$ s, respectively, responses of the frequency deviation Δf of the system subjected to $\Delta P_d = 0.01$ pu for $t \in [0\ s, 30\ s]$ and $\Delta P_d = 0$ otherwise are illustrated in Fig. 6. From this figure, Δf can be drawn back to zero after a finite time.

TABLE II
NUMBER OF CONTROL SIGNALS AND MEASUREMENTS TRANSMISSION OF LFC FOR ETM AND TTM UNDER RANDOM LOAD DISTURBANCES

Methods	ETM(h=0.05s)	ETM(h=0.1s)	TTM(h=2s)	ETM(h=2s)
NT	72	70	50	23

Although we can obtain the sampling period margin of 11.6 s or more, it is difficult to set the sampling period so large

in power system's practical operation. The possible reason is that when there is a communication failure or a physical failure of the power system, the control signal packet will be lost. In such a large sampling period ($h = 11.6$ s), if there is a continuous loss of multiple packets within tens of seconds, the stable operation of the system cannot be guaranteed. Therefore, to reduce the burden of communication networks and ensure the system can still operate stably in the presence of communication failure, it is better to choose a sampling period of $1-4$ s. On the other hand, a larger margin of the sampling period (such as 11.6 s) ensures that the system can allow five consecutive packet losses when the sampling period is set to $h = 2$ s, *i.e.*, $5h < 11.6$ s.

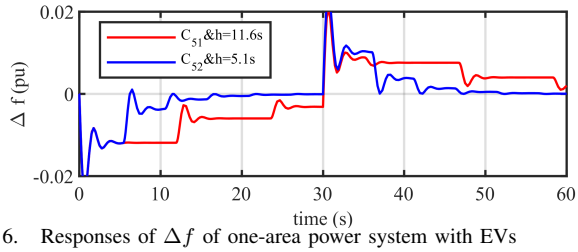

Fig. 6. Responses of Δf of one-area power system with EVs

B. Three-area power system with RESs

To further demonstrate the effectiveness of the proposed method, a three-area power system with RESs is considered to verify the robustness against load change, intermittent generation of RESs, and dynamical parametric perturbation. The parameters of this system are reported in Ref. [10], and T_{RESi} is set to 1.5s.

TABLE III
CONTROLLERS GAINS IN DIFFERENT LFC SCHEME OF THREE-AREA POWER SYSTEM

Controller	C_6 [this paper]		C_7 [11]		C_8 [15]		C_9 [10]	
	$-K_P$	$-K_I$	$-K_P$	$-K_I$	$-K_P$	$-K_I$	$-K_P$	$-K_I$
Area 1	0.0157	0.0713	-0.0250	0.1888	0.0499	0.2290	3.27e-04	0.3334
Area 2	0.0184	0.0715	-0.0396	0.2520	0.0576	0.2289	6.96e-04	0.3435
Area 3	0.0161	0.0719	-0.0308	0.2753	0.0498	0.2289	1.60e-04	0.3398

1) Controller design: Assume that the allowable sampling period and transmission delay are both set to 3 s. By setting $a = 0$, $b = 2.03$, $\lambda_{max} = 1$, $\epsilon_g = 5$, $\gamma_g = 20$, and following Algorithm 2, we can obtain the PI controller C_6 and $\lambda = 0.08$. To illustrate the effectiveness and superiority of the proposed LFC scheme, we compared the proposed scheme with the other three schemes as follows: 1) The H_∞ robust LFC scheme considering transmission delay ($\tau = 3$ s) in Ref. [11], and the proposed controller C_7; 2) The fast and discrete LFC scheme considering sampling period (h=3s) in Ref. [15], and the proposed controller C_8; 3) The robust LFC scheme considering neither transmission delay nor sampling period in Ref. [10], and the proposed controller C_9. The gains of controller $C_6 - C_9$ are shown in Table III.

TABLE IV
MARGINS OF TRANSMISSION DELAY FOR THREE-AREA LFC SCHEME UNDER SAMPLING PERIODS $h = 0.1s$, $3s$ AND $9s$

Sampling periods	h=0.1s area1/area2/area3	h=3s area1/area2/area3	h=9s area1/area2/area3
C_6	19.5/19.5/19.4	17.8/17.8/17.6	13.8/13.7/13.6
C_7	7.0/5.1/4.6	5.0/3.0/2.5	-/-/-
C_8	5.9/5.9/5.9	3.9/3.9/3.9	-/-/-
C_9	3.8/3.7/3.7	1.6/1.5/1.5	-/-/-

2) Delay margin and robust performance analysis: By using the method given in Algorithm 1, the margins of transmission delay for three-area LFC scheme with four controllers under $h = 0.1$ s, 3 s and 9 s are calculated in Table IV. Additionally, for the given four controllers, the maximal acceptable parameter uncertainties ϵ_{max} and minimal H_∞ performance index γ of area 1 in three areas are obtained under $h = 0.1$ s based on conditions 1 and 2, which are shown in Fig. 7. It can be seen from the table and the figure that the designed C_6 in this paper can provide a larger delay margin and a smaller H_∞ performance index and can tolerate larger parameter uncertainties under the same sampling period.

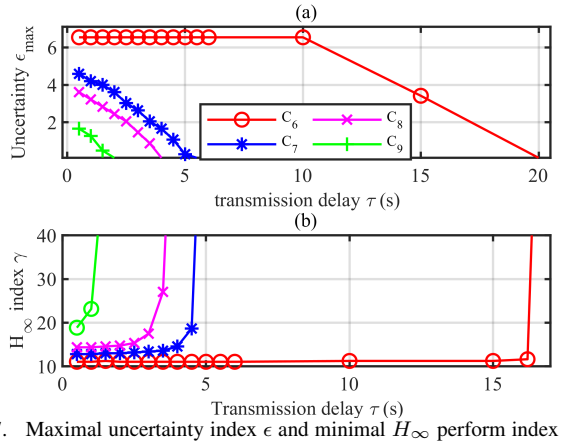

Fig. 7. Maximal uncertainty index ϵ and minimal H_∞ perform index γ with respect to delay τ under $h = 0.1s$ for Area 1 of three-area LFC scheme

3) Simulation verification: To verify the effectiveness of the proposed LFC scheme, the system equipped with the above four controllers is tested in the following two scenarios. Also, in order to show that the designed robust LFC scheme can still be effective in the presence of the important constrain, generation rate constraint, imposed by physical system dynamics. The generation rate constraint of every generator varying from -0.20 pu/min to 0.05 pu/min is considered in the following simulation.

Scenario 1*[Step changes of load and RESs]* Assume that the system is subjected to step changes of load and RESs in three areas, i.e., $\Delta P_{d1} = 0.1$ pu, $\Delta P_{d2} = 0.08$ pu and $\Delta P_{d3} = 0.06$ pu for $t \geq 0$, $\Delta P_{WS1} = 0.03$ pu, $\Delta P_{WS2} = -0.06$ pu, and $\Delta P_{WS3} = -0.05$ pu for $t \geq 0$. Under four combinations of sampling periods and transmission delays, responses of frequency deviation and control output of area 2 are shown in Fig. 8. Responses of areas 1 and 3 are similar and are omitted here. It can be seen from Fig. 8 that the designed C_6 in this paper can maintain control performance to balance the load and generations with the increase of sampling period and time delay. However, the control performances of $C_7 - C_9$ are degraded seriously, and even C_9 causes system instability at $h = 3$ s and $\tau = 3$ s.

TABLE V
ITAE FOR THREE-AREA LFC SCHEME SUBJECTED TO STEP CHANGES OF LOAD AND RESS UNDER DIFFERENT VALUES OF PV

PVs	CD($\tau = 3s$)	RTD($\tau \in [2s, 6s]$)	CD and RPL	RTD and RPL
25%	43.1	41.0	52.5	53.4
15%	42.9	40.7	52.1	52.9
5%	42.7	40.3	51.6	52.3
-5%	42.5	40.1	51.3	51.5
-15%	42.3	39.9	50.3	51.0
-25%	42.1	39.6	49.7	50.3

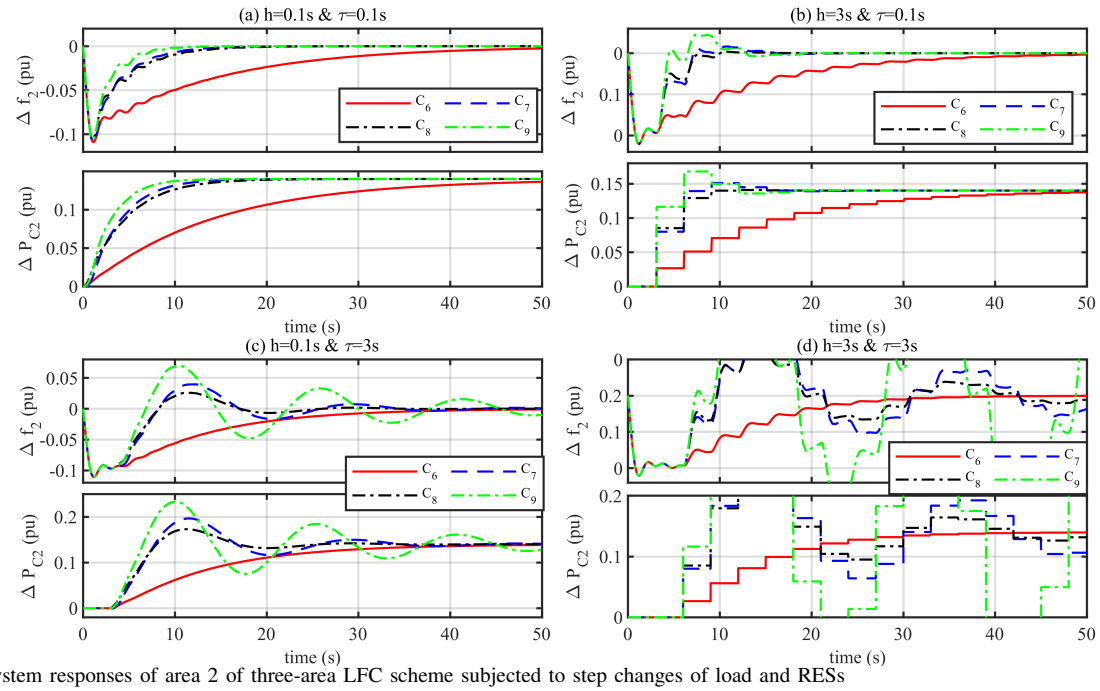

Fig. 8. System responses of area 2 of three-area LFC scheme subjected to step changes of load and RESs

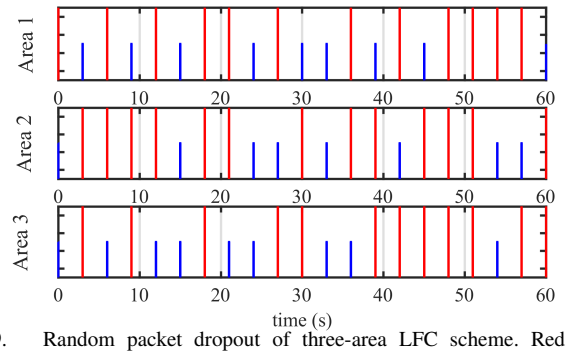

Fig. 9. Random packet dropout of three-area LFC scheme. Red line: successful transmission; blue line: packet loss

Moreover, to illustrate the robustness of controller C_6 designed for parameter variation (PV), random transmission delay (RTD), and random packet loss (RPL), we compare the control performance of the controller in the presence of above cases. To characterize the change in control performance, integral of the time multiplied absolute value of the error (ITAE) defined as ITAE $= \int_0^{T_s} t(|ACE_1| + |ACE_2| + |ACE_3|)dt$ is used to evaluate the control performance of the system. The details of RPL in three areas are shown in Fig. 9, and the RTDs in three areas change within $[2\ s, 6\ s]$. From the above delay margin analysis, when the sampling period is 9 s, the LFC system can still tolerate a large transmission delay in three areas ($\tau > 13$ s). Therefore, in the case of RPL (the maximum number n of lost packets is not more than 3, i.e. $nh \leq 9$ s) and RTD ($\tau < 13$ s), the designed controller C_6 can still maintain the control performance to balance the load and generation. When the sampling period is 3 s, the values of ITAE with $T_s = 60$ s of the system with C_6 suffering from constant delay (CD), RTD, RPL, and PVs of $T_{gki}, T_{chki}, T_{RESi}$ are given in Table V. It can be seen from Table V that the control performance is basically unchanged with the parameter varying within $\pm 25\%$ under every case of delay and sampling period. Additionally, the presence of RPL degrades the control performance to some extent due to the loss of valid control signals.

Scenario 2*[Random changes of load and RESs]* Random changes in load and RESs are shown in Fig. 10. Fig. 11 represents the responses of the frequency deviation of area 2 with controllers $C_6 - C_9$ under four combinations of sampling periods and transmission delays. Responses of areas 1 and 3 are similar and are omitted here. For better evaluating their control performance, the values of ITAE with $T_s = 300$ s for four controllers are also given in Table VI. Similar to scenario 1, from Fig. 11 and Table VI, with the increase of time delay and sampling period, the control performance of the designed C_6 in this paper is basically unchanged while the control performances of controllers $C_7 - C_9$ are degraded in different degrees and C_9 is more obviously causing the system instability.

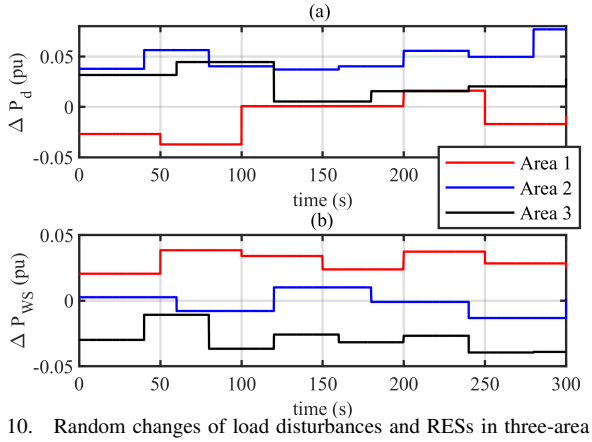

Fig. 10. Random changes of load disturbances and RESs in three-area LFC scheme

In addition, similar to scenario 1, the control performance of controller C_6 is compared in the presence of PV, RTD and RPL. Setting sampling period $h = 3$ s and $T_s = 300$ s, the values of ITAE of the system subjected to CD, RTD,

RPL, and PVs of $T_{gki}, T_{chki}, T_{RESi}$ are given in Table VII. Similar to scenario 1, controller C_6 performs strong robustness against parameter uncertainties of T_{gki}, T_{chki}, and T_{RESi} within $\pm 25\%$ under every case of delay and sampling period.

Finally, by a simple calculation, one can obtain the H_∞ performance indices of every area with controller C_6 for step and random changes of load and RESs. The values of H_∞ performance indices γ are given in Table VIII. From the calculation results in this table, it can be seen that the practical noise attenuation levels in every area under step and random changes of load and RESs are smaller than the desired level $\gamma_g = 20$, which shows controller C_6 designed in this paper can provide strong robustness against load disturbances and fluctuations of RESs.

TABLE VI
ITAE FOR THREE-AREA LFC SCHEME SUBJECTED TO RANDOM CHANGES OF LOAD AND RESS

Controller	h=0.1s $\tau = 0.1s$	h=3s $\tau = 0.1s$	h=0.1s $\tau = 3s$	h=3s $\tau = 3s$
C_6	729	742	755	744
C_7	263	301	526	1099
C_8	282	280	424	1002
C_9	209	276	770	2594

TABLE VII
ITAE FOR THREE-AREA LFC SCHEME SUBJECTED TO RANDOM CHANGES OF LOAD AND RESS UNDER DIFFERENT VALUES OF PV

PVs	CD($\tau = 3s$)	RTD($\tau \in [2s, 6s]$)	CD and RPL	RTD and RPL
25%	786	801	921	962
15%	781	796	914	955
5%	777	791	906	947
−5%	772	785	900	943
−15%	768	781	896	939
−25%	765	776	891	932

TABLE VIII
H_∞ PERFORMANCE INDICES γ FOR THREE-AREA LFC SCHEME

Load and RESs	Area 1	Area 2	Area 3
Step	0.899	1.055	1.330
Random	0.922	0.658	0.935

V. CONCLUSION

This paper has proposed a robust delay-dependent PI-based LFC scheme for a multi-area power system based on sampled-data control. Both the sampling and the transmission delay of measurements and control signals have been considered for the stability analysis and robust controller design of the LFC system. The designed LFC scheme ensures the stable operation of the power system under large transmission delay and sampling period against problems of random transmission delay and data packet loss. In addition, to cope with the load disturbances, intermittent generation of RESs, and parameter uncertainties of the power system, the EDR has been introduced as a performance index to guide the design of the LFC scheme with strong robustness. Robust performance evaluating conditions have been given to adjust the values of EDR to guarantee the designed controller with the desired robust performance of parameter uncertainties and H_∞ performance.The designed robust PI-based LFC scheme is convenient to be applied in practical LFC of power system and can be easily extended to the large-scale power systems. Two cases of power systems have been undertaken to demonstrate the effectiveness and superiority of the proposed approach.

Modern power systems are evolving towards a new generation of smart grid, where the increasing deployment of PMUs and smart metres leads to a substantial increase of measurements/control signals transmitted in an open communication network. An event-triggered communication scheme will play an important role in reducing the communication burden. Moreover, the usage of the open communication network will make the LFC scheme more vulnerable to cyber-attacks. Therefore, the next step will investigate a robust event-triggered-based LFC schemes against cyber-attacks on the base of the proposed approach.

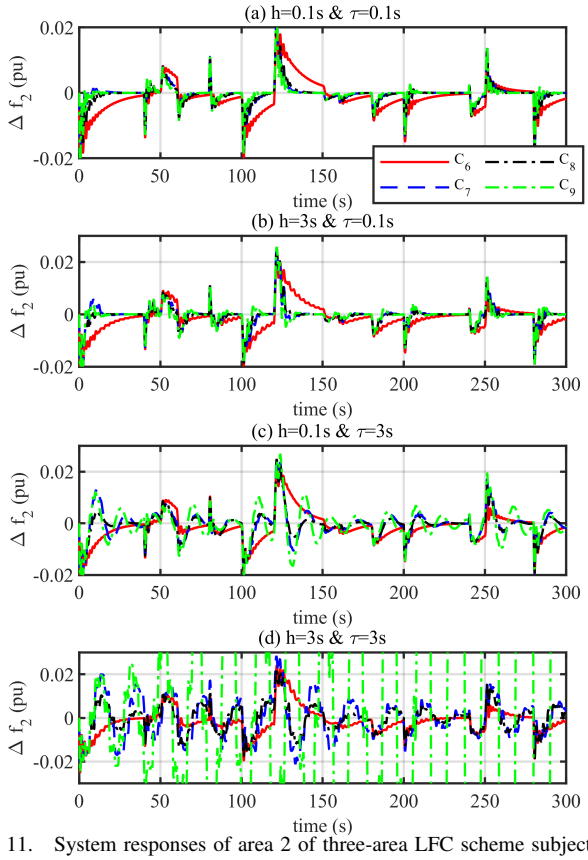

Fig. 11. System responses of area 2 of three-area LFC scheme subjected to random changes of load and RESs

VI. APPENDIX

A. Proof for Theorem 1

Choose a Lyapunov-Krasovskii functional candidate

$$V(x(t)) = V_1(t) + V_2(t) \tag{19}$$

where

$$V_1(t) = \xi_1{}^T P_1 \xi_1 + \int_{t-\tau_M}^{t} \xi_2{}^T P_2 \xi_2 ds + \int_{-\tau_M}^{0}\int_{t+\theta}^{t} \dot{x}^T(s) P_3 \dot{x}(s) ds d\theta$$

$$V_2(t) = h_{d(t)} \xi_3{}^T X \xi_3 + h_{d(t)} \int_{t_k}^{t-\tau_M} \dot{x}^T(s) Z \dot{x}(s) ds$$

with $h_{d(t)} = \eta_M - d(t)$, $d(t) = t - t_k$, $\eta_M = h_M + \tau_M$, $\xi_1 = \left[x^T(t) \quad x^T(t-\tau_M)\right]^T$, $\xi_2 = \left[x^T(s) \quad \dot{x}^T(s)\right]^T$, and $\xi_3 = \left[x^T(t-\tau_M) \quad x^T(t_k)\right]^T$. $V_1(t)$ represents the system information of transmission delay item τ_M, including one integral item and two integral items; $V_2(t)$ represents the system information of sampling period h_M and the sampling instant t_k.

Based on the free-weighting-matrix technique [36], we can obtain the following zero-equations

$$0 = 2\xi_4^T L\left(\dot{x}(t) - A_i x(t) - B_i K_i C_i x(t_k)\right) \quad (20)$$

$$0 = 2\xi^T M\left(x(t-\tau_M) - x(t_k) - \int_{t_k}^{t-\tau_M} \dot{x}(s)ds\right) \quad (21)$$

where $\xi_4 = [x^T(t),\ x^T(t_k),\ \dot{x}^T(t)]^T$ and $\xi = [x^T(t),\ x^T(t_k),\ x^T(t-\tau_M),\ \dot{x}^T(t-\tau_M),\ \dot{x}^T(t)]^T$.

Then, we can calculate the derivative of $V(x(t))$ along the trajectory of system (8); we can then use the Jensen inequality to estimate the integral items of P_3 of the derivative, and add zero-equations (20) and (21) into the derivative. This yields

$$\dot{V}(x(t)) = \frac{h_{d(t)}}{h_M}\xi^T \Xi_1 \xi + \frac{1}{h_M}\int_{t_k}^{t-\tau_M} \begin{bmatrix} \xi \\ \dot{x}(s) \end{bmatrix}^T \Xi_2 \begin{bmatrix} \xi \\ \dot{x}(s) \end{bmatrix} ds \quad (22)$$

It should be noted that $V_2(t)$ is a looped functional, and $V_2(t_k) = 0$ for $k = 0, 1, 2, \ldots$. Moreover, $V_1(t)$ is a bounded and differentiable function. Then, based on Ref. [25], if inequality conditions of (10) and (11) hold, it can guarantee $\dot{V}(x(t)) < 0$ from (22), from which it can confirm that system (8) is asymptotically stable. This completes the proof.

B. Proof for Condition 1

Lemma 1. Given appropriate dimensions matrix Q, H and symmetric matrix Σ, then

$$\Sigma + Q\Delta(t)H + H^T\Delta^T(t)Q^T < 0$$

holds for all $\Delta(t)$ satisfying $\Delta^T(t)\Delta(t) < I$, if there exists a positive scalar σ, such that

$$\Sigma + \sigma^{-1}QQ^T + \sigma H^T H < 0.$$

On the basis of proof of Theorem 1, substitute A_i and B_i with $\bar{A}_i + f(t)\Delta\bar{A}_i$ and $\bar{B}_i + f(t)\Delta\bar{B}_i$ in equation (20), and define $N_1 = \Delta\bar{A}_i$, $N_2 = \Delta\bar{B}_i K_i C_i$. One can obtain $\dot{V}(x(t))$ in equation (22) has the extra item $-2\xi_4^T L f(t) N_1 - 2\xi_4^T L f(t) N_2$. Then, based on Lemma 1 and Schur complement, if inequality conditions of (12) and (13) hold, it can guarantee $\dot{V}(x(t)) < 0$. This completes the proof.

C. Proof for Theorem 2

Define $\hat{x}(t) = x(t)e^{\lambda t}$. Since $e^{\lambda\tau(t)} \in [\rho_1, \rho_2]$ with $\rho_1 = e^{\lambda\tau_M}$ and $\rho_2 = e^{\lambda(\tau_M + h_M)}$, it can be represented in the following polytopic form:

$$\dot{\hat{x}}(t) = \sum_{j=1}^{2} \mu_j(t)\{(A_i + \lambda I)\hat{x}(t) + \rho_j B_i K_i C_i \hat{x}(t_k)\} \quad (23)$$

where $j = 1, 2$, $\mu_1(t) = (\rho_2 - e^{\lambda\tau(t)})/(\rho_2 - \rho_1)$ and $\mu_2(t) = (e^{\lambda\tau(t)} - \rho_1)/(\rho_2 - \rho_1)$. Note that the LMIs of Theorem 1 are affine in system matrices. Therefore, to guarantee asymptotic stability of system (23), we have to solve these LMIs simultaneously for the two vertices of system (23) given by $\rho_1 B_i K_i C_i$ and $\rho_2 B_i K_i C_i$, where the same decision matrices are applied. Then, based on the Theorem 1 and Ref. [26], if $\Xi_{1j} = \psi_1 + \Gamma_j + h_M\psi_2 < 0$ and $\Xi_{2j} = \begin{bmatrix} \psi_1 + \Gamma_j & -h_M\Phi_2^T M \\ * & -h_M Z \end{bmatrix} < 0$ hold, system (8) is exponentially stable with an EDR λ, where $j = 1, 2$ and $\Gamma_j = \Phi_1^T L(e_5 - (A_i + \lambda I)e_1 - \rho_j B_i K_i C_i e_2)$.

Next, define $L = [S; aS; bS]$ with tuning parameters a and b, $\hat{S} = S^{-1}$, $\hat{P}_3 = \hat{S}P_3\hat{S}^T$,$\hat{Z} = \hat{S}Z\hat{S}^T$; $\hat{P}_1, \hat{P}_2$ and $\hat{X}_i$ are defined by pre- and post-multiplying both sides of P_1, P_2 and X_i with $diag\{\hat{S}, \hat{S}\}$ and its transpose, respectively; $\hat{M} = diag\{\hat{S}, \hat{S}, \hat{S}, \hat{S}, \hat{S}\}M\hat{S}^T$; pre- and post-multiplying Ξ_{1j} by $diag\{\hat{S}, \hat{S}, \hat{S}, \hat{S}, \hat{S}\}$ and its transpose, respectively; and pre and post multiply Ξ_{2j} by $diag\{\hat{S}, \hat{S}, \hat{S}, \hat{S}, \hat{S}, \hat{S}\}$ and its transpose, respectively. Define $Y = K_i C_i \hat{S}^T$, then $\hat{\Xi}_{1j}$ and $\hat{\Xi}_{2j}$ can be obtained. $\hat{\Xi}_{1j} < 0$ and $\hat{\Xi}_{2j} < 0$ guarantee that system (8) is exponentially stable and has an EDR λ. The output feedback gains can be calculated by $K_i = Y(\hat{S}^T)^{-1}C_i^T(C_i C_i^T)^{-1}$. This completes the proof.

REFERENCES

[1] P. Kundur. *Power System Stability and Control*. New York: Mc Graw Hill, 1994.

[2] H. Bevrani. *Robust Power System Frequency Control*. New York: Springer, 2014.

[3] L. Jiang, W. Yao, Q. H. Wu, et al. "Delay-dependent stability for load frequency control with constant and time-varying delays," *IEEE Trans. Power Syst.*, vol. 27, no. 2, pp. 932-941, May 2012.

[4] S. K. Pandey, S. R. Mohanty, N. Kishor. "A literature survey on load-frequency control for conventional and distribution generation power systems," *Renewable Sustainable Energy Rev.*, vol. 25, pp. 318-334, Sept. 2013.

[5] K. Tomsovic, D. E. Bakken, V. Venkatasubramanian, et al. "Designing the next generation of real-time control, communication, and computations for large power systems," *Proc. IEEE*, vol. 93, no. 5, pp. 965-979, May 2005.

[6] H. Shayeghi, A. Jalili, H. A. Shayanfar. "Robust modified GA based multi-stage fuzzy LFC," *Energ. Convers. Manage.*, vol. 48, no. 5, pp. 1656-1670, May 2007.

[7] S. Bhowmik, K. Tomsovic, A. Bose. "Communication models for third party load frequency control," *IEEE Trans. Power Syst.*, vol. 19, no. 1, pp. 543-548, Feb. 2004.

[8] V. P. Singh, N. Kishor, P. Samuel. "Load frequency control with communication topology changes in smart grid," *IEEE Trans. Ind. Inf.*, vol. 12, no. 5, pp. 1943-1952, Oct. 2016.

[9] S. Liu, P. X. Liu. "Distributed model-based control and scheduling for load frequency regulation of smart grids over limited bandwidth networks," *IEEE Trans. Ind. Inf.*, vol. 14, no. 5, pp. 1814-1823, May 2018.

[10] D. Rerkpreedapong, A. Hasanovic, A. Feliachi. "Robust load frequency control using genetic algorithms and linear matrix inequalities," *IEEE Trans. Power Syst.*, vol. 18, no. 2, pp. 855-861, May 2003.

[11] H. Bevrani, T. Hiyama. "Robust decentralised PI based LFC design for time delay power systems," *Energy Convers. Manage.*, vol. 49, no. 2, pp. 193-204. Feb. 2008.

[12] W. Tan. "Unified tuning of PID load frequency controller for power systems via IMC," *IEEE Trans. Power Syst.*, vol. 25, no. 1, pp. 341-350, Feb. 2010.

[13] F. Yang, J. He, D. Wang. "New stability criteria of delayed load frequency control systems via infinite-series-based inequality," *IEEE Trans. Ind. Inf.*, vol. 14, no. 1, pp. 231-240, Jan. 2018.

[14] L. Jin, C. K. Zhang, Y. He, et al. "Delay-dependent stability analysis of multi-area load frequency control with enhanced accuracy and computation efficiency," *IEEE Trans. Power Syst.*, vol. 34, no. 5, pp. 3687-3696, Sept. 2019.

[15] X. C. Shang-Guan, Y. He, C. K. Zhang, et al. "Sampled-data based discrete and fast load frequency control for power systems with wind power," *Applied Energy*, vol. 259, no. 114202, Feb. 2020.

[16] S. Wen, X. Yu, Z. Zeng, et al. "Event-triggering load frequency control for multi-area power systems with communication delays," *IEEE Trans. Ind. Electron.*, vol. 63, no. 2, pp. 1308-1317, Feb. 2016.

[17] Y. Wang, I. R. Pordanjani, W. Xu. "An event-driven demand response scheme for power system security enhancement," *IEEE Trans. Smart Grid*, vol. 2, no. 1, pp. 23-29, Mar. 2011.

[18] S. Saha, M. Aldeen, C. P. Tan. "Fault detection in transmission networks of power systems," *Int. J. Elect. Power Energy Syst.*, vol. 33, no. 4, pp. 887-900, May 2011.

[19] H. Luo, I. A. Hiskens, Z. Hu. "Stability analysis of load frequency control systems with sampling and transmission delay," *IEEE Trans. Power Syst.*, 2020. Doi: 10.1109/TPWRS.2020.2980883.

[20] H. Zhang, K. Zhang, G. Xiao, et al. "Robust optimal control scheme for unknown constrained-input nonlinear systems via a plug-n-play event-sampled critic-only algorithm," *IEEE Trans. Syst., Man, Cybern., Syst.*, 2020. Doi: 10.1109/TSMC.2018.2889377.

[21] C. Peng, J. Zhang, H. Yan. "Adaptive event-triggering H_∞ load

frequency control for network-based power systems," *IEEE Trans. Ind. Electron.*, vol. 65, no. 2, pp. 1685-1694, Feb. 2018.
[22] X. Su, X. Liu, Y. D. Song. "Event-triggered sliding-mode control for multi-area power systems," *IEEE Trans. Ind. Electron.*, vol. 64, no. 8, pp. 6732-6741, Aug. 2017.
[23] L. Dong, Y. Tang, H. He, et al. "An event-triggered approach for load frequency control with supplementary ADP," *IEEE Trans. Power Syst.*, vol. 32, no. 1, pp. 581-589, Jan. 2017.
[24] H. Zhang, Y. Cai, Y. Wang, et al. "Adaptive bipartite event-triggered output consensus of heterogeneous linear multiagent systems under fixed and switching topologies," *EEE Trans. Neural Netw. Learn. Syst.*, 2020. Doi: 10.1109/TNNLS.2019.2958107.
[25] A. Seuret. "A novel stability analysis of linear systems under asynchronous samplings," *Automatica*, vol. 48, no. 1, pp. 177-182, Jan. 2012.
[26] K. Liu, E. Fridman. "Wirtinger's inequality and Lyapunov-based sampled-data stabilization," *Automatica*, vol. 48, no. 1, pp. 102-108, Jan. 2012.
[27] P. Dahiya, P. Mukhija, A. R. Saxena. "Design of sampled data and event-triggered load frequency controller for isolated hybrid power system," *Int. J. Electr. Power Energ. Syst.*, vol. 100, pp. 331-349, Sept. 2018.
[28] C. Peng, F. Li. "A survey on recent advances in event-triggered communication and control," *Inform. Sci.*, vol. 457-458, pp. 113-125, Aug. 2018.
[29] X. Liu, Y. Zhang, K. Y. Lee. "Coordinated distributed MPC for load frequency control of power system with wind farms," *IEEE Trans. Ind. Electron.*, vol. 64, no. 6, pp. 5140-5150, June 2017.
[30] H. Bevrani, M. R. Feizi, S. Ataee. "Robust frequency control in an islanded microgrid: H_∞ and μ-synthesis approaches," *IEEE Trans. Smart Grid*, vol. 7, no. 2, pp. 706-717, Mar. 2016.
[31] H. Bevrani, F. Habibi, P. Babahajyani, et al. "Intelligent frequency control in an AC microgrid: Online PSO-based fuzzy tuning approach," *IEEE Trans. Smart Grid*, vol. 3, no. 4, pp. 1935-1944, Dec. 2012.
[32] K. Liao, Y. Xu. "A robust load frequency control scheme for power systems based on second-order sliding mode and extended disturbance observer," *IEEE Trans. Ind. Inf.*, vol. 14, no. 7, pp. 3076-3086, July 2018.
[33] F. Liu, Y. Li, Y. Cao, et al. "A two-layer active disturbance rejection controller design for load frequency control of interconnected power system," *IEEE Trans. Power Syst.*, vol. 31, no. 4, pp. 3320-3321, July 2016.
[34] P. Ojaghi, M. Rahmani. "LMI-based robust predictive load frequency control for power systems with communication delays," *IEEE Trans. Power Syst.*, vol. 32, no. 5, pp. 4091-4100, Sept. 2017.
[35] V. P. Singh, N. Kishor, P. Samuel. "Improved load frequency control of power system using LMI based PID approach," *J. Franklin Inst.*, vol. 354, no. 15, pp. 6805-6830 , Aug. 2017.
[36] Y. He, Q. G. Wang, L. Xie, et al. "Further improvement of free-weighting matrices technique for systems with time-varying delay," *IEEE Trans. Autom. Control*, vol. 52, no. 2, pp. 293-299, Feb., 2007.

Xing-Chen Shangguan (S'19) received the B.S. degree in automation from China University of Geosciences, Wuhan, China, in 2016 and is pursuing the Ph.D. degree in control science and engineering from China University of Geosciences.

He is a joint Ph.D. student with the Department of Electrical Engineering and Electronics, University of Liverpool, Liverpool, U.K., from 2018 to 2020. His current research interests include sampled-data systems, time-delay systems and power systems.

Chuan-Ke Zhang (SM'19) received the B.S. degree in automation and the Ph.D. degree in control science and engineering from Central South University, Changsha, China, in 2007 and 2013, respectively.

He was a Research Associate with the Department of Electrical Engineering and Electronics, University of Liverpool, Liverpool, U.K., from 2014 to 2016. He is currently a Professor with the School of Automation, China University of Geosciences, Wuhan, China. His current research interests include time-delay systems and power systems.

Yong He (SM'06) received the B.S. and M.S. degrees in applied mathematics and the Ph.D. degree in control theory and control engineering from Central South University, Changsha, China, in 1991, 1994, and 2004, respectively.

He was a Lecturer with the School of Mathematics and Statistics, Central South University, and later a Professor with the School of Information Science and Engineering, Central South University, from 1994 to 2014. He was a Research Fellow with the Department of Electrical and Computer Engineering, National University of Singapore, Singapore, from 2005 to 2006, and the Faculty of Advanced Technology, University of Glamorgan, Glamorgan, U.K., from 2006 to 2007. He joined the China University of Geosciences, Wuhan, China, in 2014, where he is currently a Professor with the School of Automation. His current research interests include time-delay systems and networked control systems.

Li Jin (S'19) received the B.S. degree in automation from China University of Geosciences, Wuhan, China, in 2016 and is pursuing the Ph.D. degree in control science and engineering from China University of Geosciences.

She is a joint Ph.D. student with the Department of Electrical Engineering and Electronics, University of Liverpool, Liverpool, U.K., from 2018 to 2020. Her current research interests include time-delay systems, robust control, power system stability analysis and control.

Lin Jiang (M'00) received his B.S. and M.S. degrees in Electrical Engineering from the Huazhong University of Science and Technology, Wuhan, China, in 1992 and 1996, respectively; and his Ph.D. degree in Electrical Engineering from the University of Liverpool, Liverpool, ENG, UK, in 2001.

He is presently working as a Reader of Electrical Engineering at the University of Liverpool. His current research interests include the optimization and control of smart grids, electrical machines, power electronics and renewable energy.

Joseph W. Spencer received the B.Eng. and Ph.D. degrees in electrical engineering from the University of Liverpool, Liverpool, U.K., in 1981, and 1984, respectively.

He is a Professor of electrical engineering, the Director of the Centre for Intelligent and Monitoring Systems, and the Head of the School of Electrical Engineering, Electronics and Computer Science with the University of Liverpool. His current research interests include electrical power equipment and intelligent monitoring systems.

Dr. Spencer is a Committee Member of the British Standards Institution and a Fellow of the Institution of Electrical Engineering, U.K.

Min Wu (F'19) received the B.S. and M.S. degrees in engineering from Central South University, Changsha, China, in 1983 and 1986, respectively, and the Ph.D. degree in engineering from the Tokyo Institute of Technology, Tokyo, Japan, in 1999.

He was a faculty member of the School of Information Science and Engineering at Central South University from 1986 to 2014, and was promoted to Professor in 1994. In 2014, he joined China University of Geosciences, Wuhan, China, where he is a Professor in the School of Automation. He was a visiting scholar with the Department of Electrical Engineering, Tohoku University, Sendai, Japan, from 1989 to 1990, and a visiting research scholar with the Department of Control and Systems Engineering, Tokyo Institute of Technology, from 1996 to 1999. He was a visiting Professor at the School of Mechanical, Materials, Manufacturing Engineering and Management, University of Nottingham, Nottingham, U.K., from 2001 to 2002. His current research interests include process control, robust control, and intelligent systems.

Dr. Wu is a Fellow of the IEEE and a Fellow of the Chinese Association of Automation. He received the IFAC Control Engineering Practice Prize Paper Award in 1999 (together with M. Nakano and J. She).